

Gold nanoparticle synthesis: assessment of the Turkevich, green synthesis, and Good's buffer methods

Síntesis de nanopartículas de oro: evaluación de los métodos de Turkevich, síntesis verde y buffer de Good

Fátima del Rosario Balderas-Vázquez,* Diego A. Bravo-Alfaro,**
Sandra Herrera-Pérez,* Micael Gerardo Bravo-Sánchez,* Héctor Pool,***
Noé Arjona,* Gabriel Luna-Bárceñas,**, † Francisco Villaseñor-Ortega*, †

ABSTRACT: This work assesses the salient features of Au nanoparticles synthesized by bottom-up methodologies, namely the Turkevich method, the green method (quercetin), and Good's buffer method with two reducing agents (MES and PIPES). The nanoparticles' size, shape, distribution, charge, and composition were characterized using UV-Vis, FTIR, DLS, Zeta potential, TEM, and XRD. The nanoparticles from each method showed significant size, shape, and uniformity differences. Those synthesized by the Turkevich method had an average size of 28.7 nm, higher Zeta potential, and better size and spherical shape homogeneity. The green method had an average size of 25.8 nm, produced nanoparticles with high polydispersity but higher purity. In Good's buffer method, PIPES and MES resulted in larger particle sizes (37 and 43 nm) and left residues of the reducing agent. These results show that each technique offers nanoparticles with unique characteristics for potential applications.

KEYWORDS: gold nanoparticles, Turkevich method, green method, buffer method, nanoparticles characterization.

RESUMEN: Este trabajo tiene como objetivo evaluar las características destacadas de las nanopartículas de Au sintetizadas mediante metodologías de tipo *bottom-up*, específicamente el método de Turkevich, el método verde (quercetina) y el método con buffer de Good utilizando dos agentes reductores (MES y PIPES). El tamaño, la forma, la distribución, la carga y la composición de las nanopartículas se caracterizaron utilizando UV-Vis, FTIR, DLS, potencial Zeta, TEM y XRD. Las nanopartículas obtenidas por cada método mostraron diferencias significativas en cuanto a tamaño, forma y uniformidad. Las sintetizadas por el método de Turkevich presentaron un tamaño promedio de 28.7 nm, mayor potencial Zeta y mejor homogeneidad en cuanto a tamaño y forma esférica. El método verde produjo nanopartículas con alta polidispersidad pero

Received: February 12, 2025. Accepted: September 13, 2025. Published: October 23, 2025.

* Tecnológico Nacional de México en Celaya. Celaya, Guanajuato, México.

** Tecnológico de Monterrey, Institute of Advanced Materials for Sustainable Manufacturing. Querétaro, Querétaro, México.

*** Universidad Autónoma de Querétaro, División de Investigación y Posgrado, Facultad de Ingeniería. Querétaro, Querétaro, México.

• Centro de Investigación y Desarrollo Tecnológico en Electroquímica S. C. Sanfandila. Querétaro, México.

† Corresponding authors: francisco.villasenor@itcelaya.edu.mx, gabriel.luna@tec.mx



mayor pureza. En el método con tampón de Good, PIPES y MES dieron lugar a tamaños de partículas más grandes (37 y 43 nm, respectivamente) y dejaron residuos del agente reductor. Estos resultados muestran que cada técnica ofrece nanopartículas con características únicas para aplicaciones potenciales.

PALABRAS CLAVE: nanopartículas de oro, método de Turkevich, método verde, método de buffer, caracterización de nanopartículas.

Introduction

Metallic nanoparticles can be defined as a series of atoms (metallic) bound together (these particles generally contain 10⁶ atoms or fewer) and possess a size intermediate between individual atoms and aggregates large enough to be called bulk material (Ghosh and Pal, 2007). Their average particle size can vary from 1 to 100 nm, and due to this size, NPs exhibit behavior intermediates between that of a macroscopic solid and that of an atomic or molecular system, mainly due to the material's surface-to-volume ratio, quantum size effect, and electrodynamic interactions (Khan *et al.*, 2019; Scholl *et al.*, 2012). One of the main characteristics of metallic NPs is their vibrant colors due to the phenomenon known as surface plasmon resonance (SPR). When a metallic NP is small enough, it absorbs and scatters light in a particular manner due to SPR. This means that electrons on the surface of NPs can collectively oscillate in response to light, creating intense absorption in the visible spectrum region (Szunerits *et al.*, 2014; Mulvaney, 1996). For example, appropriately sized gold nanoparticles (AuNPs) have a plasmonic resonance frequency that coincides with the wavelength of red light, causing these particles to strongly absorb blue and green light while reflecting and scattering red light. As a result, a solution of gold NPs with an intense crimson-red color is obtained. This property allows us to characterize NPs using spectroscopic techniques to delve into their properties. Furthermore, this change in reflectance due to SPR can be measured and utilized in various applications such as biomolecule detection, molecular interaction analysis, thin film studies, and biosensors (Jamkhande *et al.*, (2019).

Several techniques are employed to fabricate metallic NPs, which are classified into two general methods: bottom-up and top-down. The former is based on the formation of nanoparticles from smaller molecules, such as the assembly of atoms or molecules into small particles. In this method, nanostructured building blocks of the nanoparticles were formed and then assembled to produce the final nanoparticle (Pacioni *et al.*, 2015). On the other hand, in the top-down method, nanoparticle preparation is based on reducing the starting material size through various physical and chemical treatments (Meyers *et al.*, 2006). The bottom-up method allows the production of smaller sized gold nanoparticles (AuNPs), thus making it one of the most widely used techniques. Most of these techniques are based on reducing chloroauric acid (HAuCl₄) precursors using reducing agents. There are various processes for

synthesizing different AuNPs, each resulting in multiple nanoparticles with different sizes and shapes (Niu *et al.*, 2007; Rahme and Holmes, 2015) and hence different properties. Consequently, a comparative analysis of the resulting NP from some of these methods is necessary to establish the appropriate technique depending on the purpose of the nanoparticle.

As mentioned earlier, various types of metallic precursors (typically complex metal ions) are used for nanoparticle synthesis in aqueous solution, with inorganic salts, thiols, carboxylates, phosphines, or amines among the stabilizers employed. One of the earliest methods described for AuNP formation is the Turkevich method. This method involves obtaining nanoparticles by reducing chloroauric acid (HAuCl_4), where gold ions Au^{+3} is reduced to neutral gold atoms A^0 by a reducing agent, sodium citrate (Turkevich *et al.*, 1951). In this method, the growth mechanism involves the rapid reduction of the precursor and the immediate formation of stable seed particles with a radius of 1.5 nm. Subsequently, the precursor attaches and continues to reduce the electric double layer of these newly formed seeds. Although NPs from this method can be easily functionalized, the quantity of seeds formed at the start of the reaction is critical for the final properties of the AuNPs; thus, this method is sometimes not highly reproducible, posing some challenges in its selection (Kettemann *et al.*, 2016).

On the other hand, the green method is a relatively new approach to synthesizing gold nanoparticles, involving the production of gold nanoparticles using chloroauric acid as a precursor and employing some naturally derived flavonoids such as quercetin as a stabilizing agent. Quercetin is a flavonol with antioxidant properties abundant in fruits and vegetables, acting as a protector against reactive oxygen species by neutralizing free radicals such as superoxide anions, nitric oxide, and peroxy nitrates, among others (Vergara-Castañeda *et al.*, 2019). Using natural stabilizing agents allows for an environmentally safe NP process, and green methods yield biocompatible nanoparticles suitable for biological applications (Devendiran *et al.*, 2016).

Another method utilized in this article is Good's buffer method, which is named after using at least one of the 20 solutions selected and described by Norman Good. It's called "Good's buffer" (Good *et al.*, 1966). Most of these solutions are novel zwitterionic compounds prepared and tested by Good and colleagues. In this project, PIPES (piperazine-N, N'-bis) and MES (2-(N-morpholino) ethanesulfonic acid) buffers were used as reducing agents (Ahmed *et al.*, 2016).

This study compares different methodologies for synthesizing gold nanoparticles to determine size, shape, and density variations. We seek to evaluate how changes in reducing agents, temperature, and agitation affect these characteristics. This information is crucial for selecting the most suitable synthesis method to obtain nanoparticles with specific factors relevant to medicine, food, and chemical synthesis applications. Detailed knowledge of the obtained nanoparticles will optimize their use and efficiency in ap-

plying particular ligands in future experiments.

Materials and methods

Materials

Chloroauric acid trihydrate ($\text{HAuCl}_4 \bullet 3\text{H}_2\text{O}$) with a purity $\geq 99.9\%$, piperazine-N, N'-bis(2-ethanesulfonic acid) (PIPES), 2-(N-morpholino) ethanesulfonic acid (MES), and quercetin were obtained from Sigma-Aldrich (St. Louis, MO, USA). Distilled water and deionized water were acquired from TQE Servicios (San Luis Potosí, Mexico).

Nanoparticle synthesis

Turkevich method

To synthesize gold nanoparticles using the Turkevich method, 10 mL of a 1 mM HAuCl_4 solution was combined with 1 mL of 38.8 mM sodium citrate. This mixture was transferred to an oil bath and heated to 160 °C for 20 minutes, constantly stirring. The formation of nanoparticles was indicated by a color change to a crimson red hue (Turkevich *et al.*, 1951)

Green method

The green nanoparticle production method involved mixing 23.75 mL of a 1 mM HAuCl_4 solution with 1.25 mL of a 50 μM quercetin solution in a beaker. This mixture was stirred in a water bath at 40 °C for 5 hours. The color change to reddish-brown signaled the formation of the nanoparticles (Vergara-Castañeda *et al.*, 2019).

Good's buffer method

PIPES buffer

This method involved adding 4 mL of 100 mM PIPES buffer to a beaker, which was then stirred and heated in an oil bath at 100 °C. Subsequently, 1 mL of 20 mM HAuCl_4 solution and 36 mL of deionized water were added. The mixture was stirred for 30 minutes. The color change to crimson red in the solution indicates the formation of nanoparticles (Ahmed, S.R *et al.*, 2016).

MES buffer

To carry out this methodology, 4 mL of MES buffer (100 mM) was added to a beaker, stirred, and heated in an oil bath at 100 °C. Next, 1 mL of a 20 mM HAuCl_4 solution was added and mixed with 36 mL of deionized water. The solution was stirred for 20 minutes and maintained at 100 °C. The change in the solution's color to crimson red indicates the formation of nanoparticles (Ahmed, S.R *et al.*, 2016).

Characterization of nanoparticles

The synthesized nanoparticles were characterized using various techniques.



Firstly, the size and morphology of the synthesized nanoparticles were studied using transmission electron microscopy (TEM), and their intrinsic properties were identified for surface plasmon resonance by UV-visible spectroscopy. The nanoparticle diameter was estimated using dynamic light scattering (DLS) and nanoparticle dispersion stability through zeta potential measurement. The sample's structure and chemical nature were analyzed by Rigaku Ultima-IV diffractometer with a for the XRD and Fourier-transform infrared spectroscopy (FTIR).

UV-VIS spectroscopy

The UV-VIS characterization of the solutions of synthesized nanoparticles using the Turkevich, green, and Good's buffer methods was performed using a Thermo SCIENTIFIC MULTISKAN 60 spectrophotometer, employing an Elisa plate in the range of 1000 to 200 nm.

TEM

The morphological characterization of the nanoparticles obtained using the different proposed methods was carried out using the JEOL JEM-1010 transmission electron microscope, USA, under an acceleration voltage of 80-100 kV. For sample preparation, 1 mL of each sample was taken and deposited onto a copper grid on a glass slide for observation, spread with a rod, and allowed to dry for 15 minutes. The size and shape of the nanoparticles in different fields were analyzed randomly using image-J software.

Zeta potential

Zeta potential analysis was performed using the Zetasizer Nano ZS, Malvern Inst., USA. An aliquot of approximately 3 mL of each sample was taken, and the reading was conducted on the computer. Measurements were performed in triplicate.

DLS

A dynamic light scattering (DLS) instrument, Zetasizer Nano ZS, Malvern Inst., USA, was used to measure particle size and diameter distribution. Measurements for each nanoparticle solution were conducted in triplicate.

X-ray diffraction (XRD)

X-ray diffraction measurements were performed using a Rigaku Ultima-IV diffractometer with a temperature chamber (Rigaku HT-1500). The samples were analyzed in powder form.

FTIR

Samples were dried at 40 °C for 48 hours before being analyzed using Fourier-transform infrared spectroscopy by diffuse reflectance. The infrared spectrum was obtained from 500 to 400 cm^{-1} with 24 scans and a resolution of 4



cm^{-1} . The equipment used was an FTIR spectrophotometer by PERKIN EL-MER, model GX 51150.

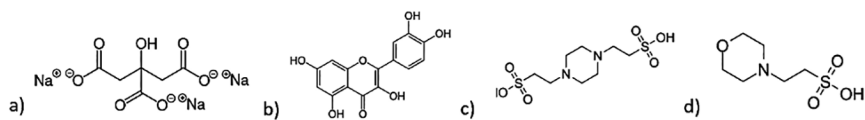
Statistical analysis

The analysis of variances and the comparison of means by the Tukey test ($p < 0.5$) were analyzed using the statistical software STATGRAPHICS Centurion XVI®.

Results

Chemical structure of each precursor is showed in figure 1, each of them has different functional groups, which gives rise to a variety of types of bonds during nucleation resulting from the different electronegativity values that each element has when interacting. Each reducing agent acts as a stabilizing or dispersing agent, which adheres to the surface of the newly formed nanoparticles, preventing or promoting the aggregation of the nanoparticles during the reaction. As for sodium citrate, which is the reducing agent in Turkevich's method, it has sodium atoms in its terminal chains. When the oxidation-reduction reaction occurs with chlorine atoms, negative charges are generated that prevent the aggregation of the nanoparticles, controlling size and shape. In contrast to what is observed in the green method where quercetin is a flavonoid and has hydroxyl groups (-OH) in its structure that form hydrogen bonds. As result the flavonoid decreases its solubility and reaction speed, therefore there is a great-

FIGURE 1. Chemical structures of the reducing agents of the methodologies used for the synthesis of nanoparticles. a) Structure of sodium citrate as a reducing agent in the Turkevich method; b) structure of quercetin as a reducing agent for the green method; c) and d) are the reducing agents PIPES and MES respectively for the Good's buffer method.



Source: Author's elaboration.

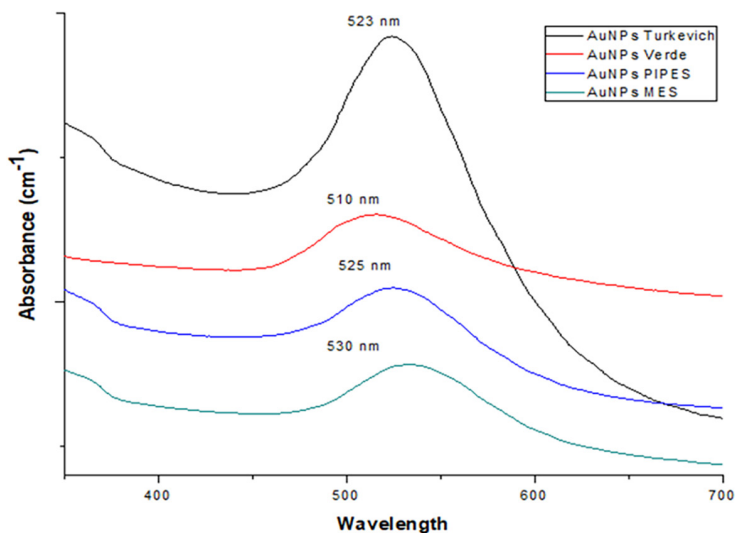
er number of residues that adhere to the surface of the nanoparticle, preventing nucleation from continuing, having smaller particles.

UV-Vis

The absorption spectra of the nanoparticles obtained by the three methods absorbed a visible range between 520-550 nm (figure 2). The absorbed wavelengths in all the AuNPs prepared in this study correspond to the wavelength of the blue-green portion of light, hence reflecting the wavelengths of red light, explaining the reddish coloration of the AuNP solutions. When light hits a gold nanoparticle, electrons on the nanoparticle's surface can col-

lectively oscillate in response to the electric field of the incident light. This phenomenon is known as surface plasmon resonance. The frequency at which these electrons oscillate most efficiently depends on the size and shape of the nanoparticle. When the frequency of the incident light matches the resonance frequency of the surface plasmon of the gold nanoparticle, strong light absorption occurs at that wavelength (520-550 nm in this case). This is because the energy of the light is efficiently transferred to the surface electrons of the nanoparticle, leading to significant excitation of the surface plasmons (Jain, P. K. *et al.*, 2007). Therefore, the size and shape of the gold

FIGURE 2. UV-visible for nanoparticles obtained for different methods.



Source: Author's elaboration.

nanoparticles determine the wavelength of visible light they absorb most efficiently. Thus, this plasmon provides information about the nanoparticles' size, shape, and aggregation (Krajczewski *et al.*, 2017).

On the other hand, the reduction rate of each method depends on the reducing agent used, temperature, and synthesis time. A surface plasmon has been identified between 450 nm and 700 nm for gold nanoparticles, depending on the nanoparticle size, concentration, and anisotropy (Huang and El-Sayed, 2010).

The surface plasmon of the nanoparticles synthesized by Turkevich exhibited a strong absorption signal near $\lambda = 523$ nm (particle size approximately 15-30 nm). This intensity in the absorption signal could provide information about the nanoparticle's shape, as spherical nanoparticles tend to be more efficient in light absorption. This has been previously reported,

stating that the nanoparticle's shape can influence absorption efficiency at specific wavelengths. Different geometric shapes have different surface plasmon resonance modes, which can affect how they interact with incident light. Spherical AuNPs have a well-defined surface plasmon resonance and efficiently absorb light at specific wavelengths that match their resonance (Murphy *et al.*, 2005).

On the other hand, the band obtained by the green method exhibited a decrease in intensity and absorption at approximately $\lambda = 510$ nm (particle size between 10-20 nm), resulting from smaller nanoparticles and a slightly anisotropic shape. Regarding Good's buffer method, the intensity of the plasmon in both spectra was lower than that of Turkevich but marginally higher than that obtained by the green method, indicating a good nanoparticle concentration. Similarly, the plasmons slightly shifted to the right at approximately $\lambda = 525$ nm for PIPES and $\lambda = 530$ nm for MES.

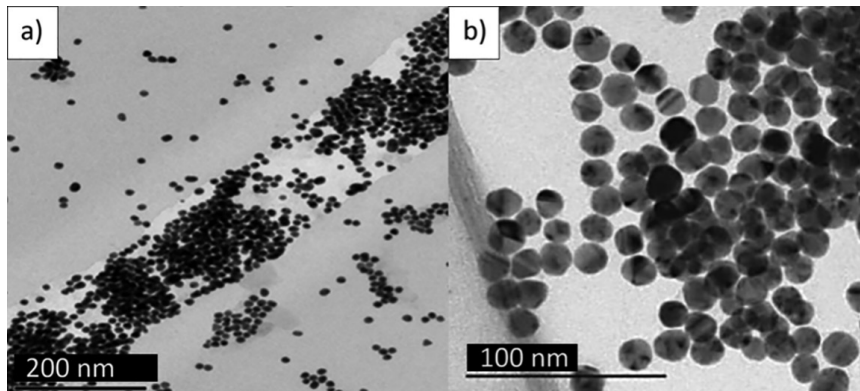
The size of AuNPs determines the frequency of resonance of the surface plasmon. Generally, as the particle size increases, the resonance wavelength of the surface plasmon also increases. This means that larger nanoparticles have resonance at longer wavelengths. For example, smaller gold nanoparticles tend to resonate in the visible range of the electromagnetic spectrum (approximately between 500 and 700 nm), while larger nanoparticles may resonate in the near infrared (Huang and El-Sayed 2010; Jain *et al.*, 2006). Based on the results obtained, we can estimate that nanoparticles fabricated by the MES method should have the largest particle diameter, followed by those made by the PIPES method, then those prepared by Turkevich, and finally by the green method.

However, these results should be interpreted with caution as the shape of the gold nanoparticle also affects its surface plasmon resonance. For example, as mentioned earlier, spherical AuNPs have a well-defined surface plasmon resonance and can efficiently absorb light. However, other shapes, such as nanorods, nanocubes, or nanostars, have surface plasmon resonances that can be tuned by changing their geometric dimensions. Therefore, it is possible to tune the surface plasmon resonance by changing the shape of the gold nanoparticles (Millstone *et al.*, 2009). In this regard, absorption can also give us an idea of the geometric shape of the AuNPs.

TEM (transmission electron microscopy)

Samples of gold nanoparticles were analyzed using TEM, and micrographs were obtained to determine their structure and morphology. Figure 3(a) shows the 200 nm micrograph of the nanoparticles obtained using the Turkevich method, where a predominance of nano-spherical structure, a homogeneous distribution of size and shape, and a slight accumulation of nanoparticles are observed. Meanwhile, in figure 3(b) at 100 nm, the size of a group of nanoparticles ranging between 15 and 9 nm is shown. With this method, we can deduce that the formed nanoparticles possess a spherical

FIGURE 3. Micrographs of gold nanoparticles obtained by Turkevich's method: a) micrograph at 200 nm, and, b) micrograph at 100 nm.

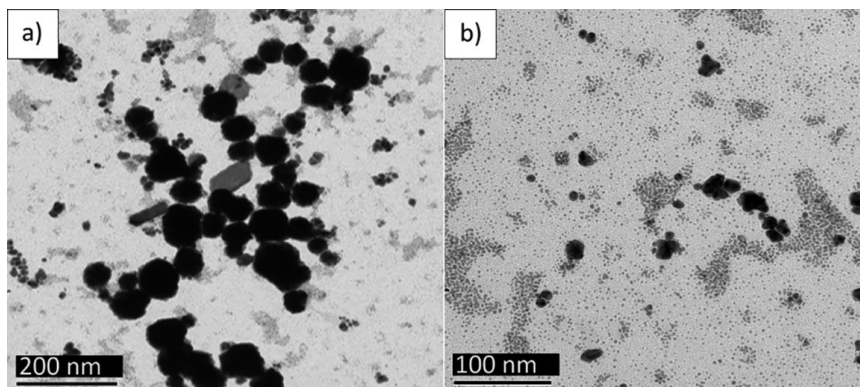


Source: Author's elaboration.

shape and average diameters below 30 nm.

The spherical shape of the NPs has certain advantages over other forms; for example, spherical AuNPs exhibit a well-defined surface plasmon resonance in the visible range of the electromagnetic spectrum, making them useful in imaging applications, optical sensors, and photothermal therapy. Additionally, they can be easily modified with different molecules, such as targeting agents, contrast agents, or therapeutic agents. This allows for the adaptation of nanoparticles for specific applications, such as drug delivery or biomolecule detection (Dreaden *et al.*, 2012). Figure 4 shows the micrographs of the nanoparticles obtained through green synthesis, where the nanoparticles were more heterogeneous than those synthesized by the Turkevich method. In figure 4a, a higher number of nanoparticle agglomera-

FIGURE 4. Micrographs of gold nanoparticles obtained by green's method: a) micrograph at 200 nm, and, b) micrograph at 100 nm show small nanoparticles.



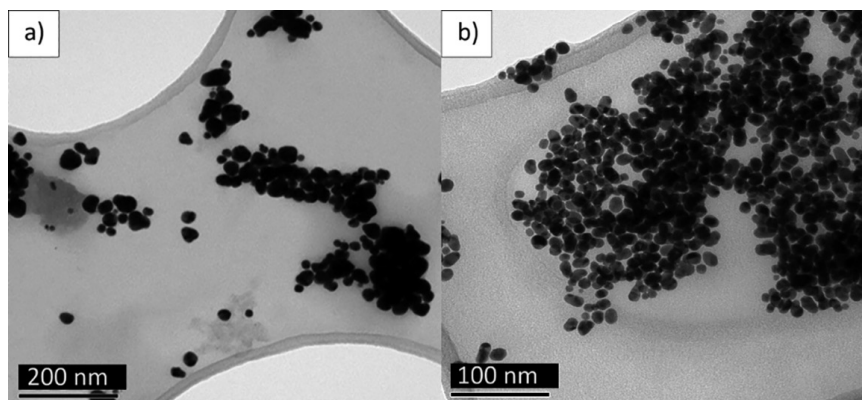
Source: Author's elaboration.

tions was found.

Meanwhile, in 4b, at 100 nm, it was observed that the size of the smaller nanoparticles varied between 1.43 nm and 14.78 nm. The presence of such small and abundant particles may result from small nuclei that fail to increase their diameter. It is important to recall that in the bottom-up formation scheme of AuNPs, reduced gold ions aggregate to form gold nanoparticle nuclei during nucleation. These nuclei are small accumulations of gold atoms that represent the starting point for the subsequent growth of nanoparticles, which can reach a nanometer in diameter (Polte, 2015).

Once the nuclei have formed, gold nanoparticles begin to grow from them by the addition of additional gold atoms. Nucleation and growth con-

FIGURE 5. Micrographs of gold nanoparticles obtained by the Good's buffer method with PIPES as reducing agent: a) nanoparticles are observed at 200 nm; b) nanoparticles are observed at 100 nm.



Source: Author's elaboration.

tinue until a balance between the nucleation and growth rate is reached, resulting in gold nanoparticles of controlled size and shape (Oliveira *et al.*, 2023).

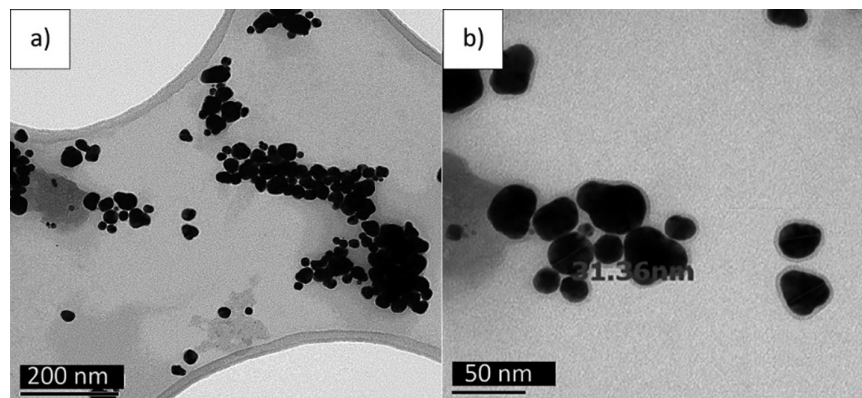
The ability of gold nuclei to grow and form nanoparticles depends on the availability of reduced gold ions in the solution. The reducing agent provides the necessary electrons to reduce the gold ions in the solution and form the initial nuclei. If the concentration of the reducing agent is insufficient or its activity decreases prematurely, the gold nuclei may cease to grow and efficiently form nanoparticles. This can lead to the formation of small nuclei or incomplete nucleation, producing gold nanoparticles of reduced size or with a broader size distribution (Jana *et al.*, 2001). The above may explain the heterogeneity in the particles by the green method and the presence of so many small particles. Therefore, quercetin seems not to be a good reducing agent to produce uniform nanoparticles. Remember that quercetin is highly hydrophobic and very poorly soluble in aqueous media (Abraham and Acree,

2014), which could be an important factor in its use as a reducing agent. Micrographs of nanoparticles obtained using Good's buffer method with PIPES as a reducing agent are shown in figures 5a and 5b. The nanoparticles do not have a defined and homogeneous spherical shape. Additionally, the particle size is larger than that obtained with the Turkevich and green methods, with a size range of approximately 20 to 40 nm. This confirms the information obtained by UV-Vis, where the spectrum obtained is absorbed at longer wavelengths, indicating a larger nanoparticle size.

This synthesis presents some nanoparticle clusters, indicating that PIPES as a reducing agent provides less reaction stability than sodium citrate for the Turkevich method. This results in the solution containing larger nanoparticles, which tend to form clusters and agglomerates.

The micrographs of the nanoparticles obtained with MES as a reducing agent are shown in figure 6a. In this case, the nanoparticles are larger than those obtained by the other proposed methods, and their shape is semi-spherical, presenting slight aggregation in certain regions of the analyzed sample. Figure 6b specifies that the size of the nanoparticles is around 30 nm. A certain percentage of nanoparticles are spherical; some are slightly

FIGURE 6. Micrographs of gold nanoparticles obtained by the Good's buffer method with MES as reducing agent: a) nanoparticles are observed at 200 nm; b) nanoparticles ranging from 28 nm.



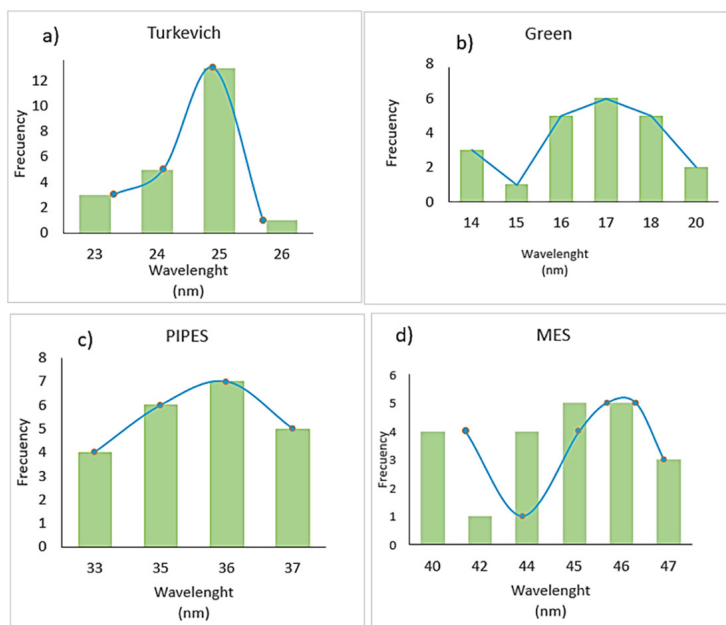
Source: Author's elaboration.

oval, and others are somewhat triangular. Overall, Good's buffer method with two reducing agents had a more irregular shape and was larger than those obtained by Turkevich and the green method.

Figure 7 shows the size distribution histograms for the nanoparticles obtained by the Turkevich method (a) and the green method (b), both obtained by TEM. In the histogram of part (a), greater size uniformity is observed, presenting a curve with greater symmetry around the average of 25 nm. This indicates that the stirring conditions, temperature, and concentra-

tion of the reducing agent considerably influence the uniformity of the data distribution. In contrast, in the distribution graph corresponding to the synthesis by the green method (figure 7b), a central bell-shaped distribution as in Turkevich is not observed. Although most nanoparticles in the green method present an average size of 17 nm, there is a large variation, as two modes are observed in the same graph, indicating that there are two groups of different sizes within the solution, with the second group predominating

FIGURE 7. TEM analysis of gold nanoparticles: a) synthesized by Turkevich method; b) gold nanoparticles synthesized by the green method; c) PIPES method; d) MES method.



Source: Author's elaboration.

in the synthesis.

This can be corroborated with the DLS results, where the PDI resulting from the green method was higher compared to the Turkevich method.

Regarding the nanoparticles obtained by the Good's buffer method with PIPES and MES as reducing agents (figure 7c and d, respectively), the graphs show that although these methods shared similar stirring times and temperatures, the size was mainly influenced by the type of reducing agent, which plays a key role in the nucleation of the nanoparticles, resulting in differences in both size and shape.

While the nanoparticles synthesized with PIPES exhibit size uniformity with an average size of 35 nm (see table 1), the nanoparticles obtained with

TABLE 1. Polydispersity index and particle sizes obtained in nanoparticles prepared by different methods.

Method description	Particle size (nm) measurement by DLS	Particle size (nm) measurement by TEM	PDI
Turkevich	28.73 ± 0.57 ^b	25 ± 0.78	0.38 ± 0.013 ^d
Green	20 ± 1.81 ^a	17 ± 1.59	0.61 ± 0.013 ^a
MES	43.55 ± 0.55 ^d	35 ± 1.34	0.41 ± 0.009 ^c
PIPES	37.53 ± 0.87 ^c	44 ± 2.32	0.44 ± 0.013 ^b

The values correspond to the mean ± SD (n = 3). Values with at least one letter in common are not significantly different p < 0.05.

Source: Author's elaboration.

MES show a more varied size distribution, reflected in the graph by a dispersed bell curve. Nevertheless, both methods yielded PDI values between 0.41 and 0.44 in the DLS analysis, suggesting moderate polydispersity.

In the green methodology, nanoparticle sizes are smaller and present greater size dispersion, evidenced by a broader bell curve. This distribution is more uniform compared to methodologies that produce larger nanoparticles (PIPES and MES).

Table 1 summarizes the characteristics obtained through TEM analyses, as well as their comparison with DLS, where smaller sizes are observed than those reported by DLS. However, differences of around 10 nm between nanoparticle sizes measured by TEM and DLS are common and expected, as both techniques measure different properties: TEM determines the direct physical size of the particles in a dry state, while DLS measures the hydrodynamic radius, which includes the solvent layer and possible molecules adsorbed on the surface. Additionally, DLS is less precise in distinguishing small size variations when the distribution is polydisperse, which can generate discrepancies with TEM results.

Finally, the differences in size and shape between methods may be related to the chemical structure of the reducing agents used.

Zeta potential

The colloidal stability of the synthesized nanoparticles was evaluated using zeta potential (ZP). ZP, also known as electrokinetic potential, is the potential at the slipping plane of a colloidal particle moving under an electric field. The electric potential of a surface is the amount of work required to bring a unit of positive charge from infinity to the surface without any acceleration. In this sense, ZP represents the potential difference between the electrical double layer of electrokinetically mobile particles and the surrounding dispersed phase layer at the slipping plane (Bhattacharjee, S. 2016). Commonly, ZP is associated with the stability of nanosystems over time, with ranges of |0-10| mV,

|10–20| mV, |20–30| mV, and > |30| mV considered highly unstable, relatively stable, moderately stable, and highly stable systems, respectively (Patel and Agrawal, 2011). As a result, negative values were observed for all methods, suggesting that nanoparticles may adhere to the surface ions of the reducing agents for each method. The nanoparticles synthesized using the Turkevich method obtained an average value of -38.65 mV (table 2), statistically significantly higher than those obtained by other methods ($p < 0.05$), indicating that these nanoparticles have high stability and are less prone to aggregate and precipitate. The green method, as well as Good's buffer method with PIPES and MES as reducing agents, showed average values between -26 and -28 mV, values that did not show a significant difference between them ($p > 0.05$), indicating moderate stability according to the previously proposed scale.

There are many factors that can interfere with the zeta potential of AuNPs, such as surface charge, electrolyte concentration, and the presence of stabilizing agents. Some authors have reported that larger AuNPs tend to have a lower absolute value of zeta potential, while smaller NPs may have a higher absolute value of zeta potential. This is because larger nanoparticles have lower electrophoretic mobility due to their larger size and mass, resulting in a lower zeta potential. On the other hand, smaller gold nanoparticles have higher electrophoretic mobility due to their smaller size and mass, which can result in a higher zeta potential (Nakatuka *et al.*, 2015; Zuki *et al.*, 2019). However, contradictorily, it has been observed that smaller nanoparticles tend to agglomerate more easily (Wang *et al.*, 2019). Therefore, the influence between particle diameter and ZP is still not clear. In the present work, the green method obtained the smallest particle diameters, but with high polydispersity, indicating the presence of larger and heterogeneous particles. Meanwhile, the Turkevich

TABLE 2. Measurement of the average Z potential of the nanoparticles obtained.

Method description	Z Potential (mV)
Turkevich	-38.65 ± 1.25^a
Green	-28.4 ± 0.71^b
MES	-26.75 ± 0.93^b
PIPES	-27.68 ± 0.94^b
The values correspond to the mean \pm SD ($n = 3$). Values with at least one letter in common are not significantly different $p < 0.05$.	

Source: Author's elaboration.

method achieved the second smallest particle sizes with low polydispersity, indicating more uniform and smaller nanoparticles. Therefore, perhaps particle size does have an influence on the final zeta potential of the nanosystems.

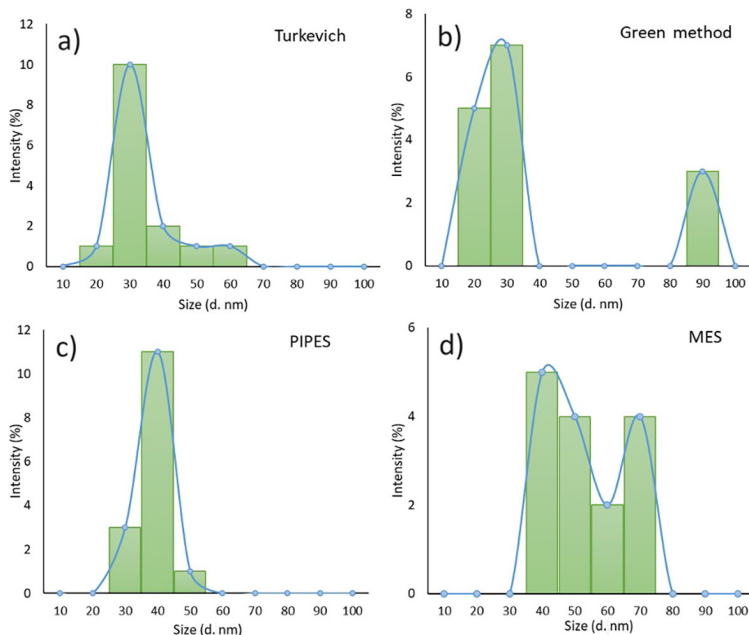
DLS

Dynamic light scattering technique was used to provide more detailed information on the size distribution of the nanoparticles produced by each method. The nanoparticles obtained by the Turkevich method had a spherical shape (as observed by TEM), with an average diameter of approximately 28.7 nm. Figure 8 presents the size distribution histograms for the nanoparticles obtained by the Turkevich method a) and for the green method b).

In histogram a), the highest mode was observed near 30 nm, which corresponds to the average diameter reported by the equipment (28.7 nm); however, particles with distributions ranging from 10 nm to 70 nm were also obtained. The polydispersity index (PDI) describes a distribution's "nonuniformity" degree. This value is calculated based on the width of the particle distribution. The range is from 0.0 (a perfect uniform sample) to 1.0 (a highly polydisperse sample with multiple particle sizes) (Danaei *et al.*, 2018). In this regard, the AuNPs fabricated by the Turkevich method showed the lowest PDI among all the analyzed methods (0.38) (see table 1), suggesting a good particle size distribution, i.e., a more homogeneous system in terms of diameters. Therefore, it is possible to consider that for the Turkevich method, the agitation speed and the reaction time were ideal for achieving greater homogeneity in the nanoparticles.

Regarding the green method, the average size of the nanoparticles was approximately 20 nm, with slightly less homogeneity in size distribution (PDI = 0.61), which aligns with observations made by TEM. Additionally, according to figure 6b, we can observe a bimodal distribution, with one mode near 30 nm and another near 90 nm. This could be attributed, as mentioned earlier, to the inefficient action of the precursor agent and the temperature and reaction time. With a much lower temperature than the Turkevich technique, the nucleation time was longer, which could be a factor influencing smaller nanoparticles. Regarding the action of the reducing agent (quercetin in this case), it has a larger structure than sodium citrate (used in the Turkevich method), leading to a slower nucleation process under these conditions, not to mention its high hydrophobicity. It is necessary to note that the values obtained by DLS in the green method are higher than those observed by TEM since equipment used for determination can only detect particles larger than 3 nm. In comparison, nanoparticles as small as TEM observed 1 nm.

For nanoparticles obtained using Good's buffer method with PIPES and MES as reducing agents (figure 8c and 8d), the average size is larger than that obtained in the previous synthesis methods, with an average average diameter of 37.5 nm for PIPES. For MES, the size was slightly larger (43.55 nm). The results can be seen in table 1. The differences in size between both methods may be due to the agent's speed, reaction time, and temperature, which are like the Turkevich method. Additionally, the reducing agent may have an affinity with other chains of the same agent, potentially causing conglomerates to form, resulting in larger nanoparticles.

FIGURE 8. DLS analysis of gold nanoparticles: a) synthesized by Turkevich method; b) gold nanoparticles synthesized by the green method; c) PIPES method; d) MES method.

Source: Author's elaboration.

As seen in table 1, the PDI varies in each nanoparticle solution. Higher PDI values indicate less stability in the PIPES and MES solutions. Nanoparticles obtained using PIPES and MES as reducing agent had the greatest size variations compared to Turkevich. However, the methodologies have different synthesis conditions, so it can be inferred that the variation in size and polydispersity is due to the efficiency of the reducing agent.

Table 1 shows notable differences in the standard deviation (SD) values associated with the particle size and the polydispersity index (PDI) obtained by the different synthesis methods evaluated. These values allow us to estimate the degree of dispersion of the data and, therefore, the uniformity of the nanoparticles generated. Regarding the particle size measured by DLS, the green method presented the highest standard deviation (± 1.81 nm), which reflects a high variability in the size of the nanoparticles obtained through this process. This suggests that this method generates particles with lower homogeneity compared to the other methods evaluated. In contrast, the MES (± 0.55 nm) and Turkevich (± 0.57 nm) methods showed the lowest standard deviations, indicating a more uniform size distribution. The PIPES method presented an intermediate value (± 0.87 nm), which shows a moderate dispersion.

Regarding measurements by transmission electron microscopy (TEM), a similar behavior was observed. The PIPES method showed the highest standard deviation (± 2.32 nm), followed by Green (± 1.59 nm) and MES (± 1.34 nm), confirming a more heterogeneous distribution in these cases. In contrast, Turkevich again showed the lowest dispersion (± 0.78 nm), which reinforces its ability to produce nanoparticles with a more controlled and constant size.

As expected, the sizes of nanoparticles analyzed by TEM and DLS were different, with those analyzed by DLS being larger since this technique measures the hydrodynamic diameter, which includes not only the core of the nanoparticle but also ligands or possible aggregates, while TEM measures the real physical size of the nanoparticles, the images obtained allow us to directly observe the core of the particle, its shape and size distribution, since the measurements are carried out in a dry state and do not consider the liquid environment, nor interactions between particles. The contrast of the results of both techniques avoids the bias that the DLS technique makes towards larger particles. Both techniques are complementary, and their joint use allows a more complete and reliable characterization of nanoparticles. These results reflect that synthesis methods significantly influence the size dispersion of nanoparticles. Turkevich method stands out for offering greater consistency in particle size, while the green method, despite its sustainable approach, presents greater variability, which may limit its applicability in contexts where monodispersity is a critical requirement.

Data obtained by TEM and DLS was reflected in the UV-vis analysis when the surface plasmon shifts of each method were observed. Those smaller nanoparticles moved slowly as they had little surface area, such is the case of the nanoparticles from the green method that have a wavelength of 510 nm, while those obtained by the Good's buffer methods have a greater displacement at being able to reflect a greater amount of light because they are larger nanoparticles.

The average number of gold atoms per individual NP was calculated from the average size data of the nanoparticles obtained from TEM and DLS. Spherical shape was predominant in all synthesis methods, so assuming that the density of the nanoparticles is the density of gold and that the structure is uniform, the number of atoms (N) calculated for the synthesis was determined using the following equation:

$$N = \frac{\pi \rho D^3}{6M} = 30.9D^3 \quad (1)$$

Where:

ρ : density of gold assuming a uniform structure, 19.3 g/cm^3

D: average diameter of the gold nanoparticles

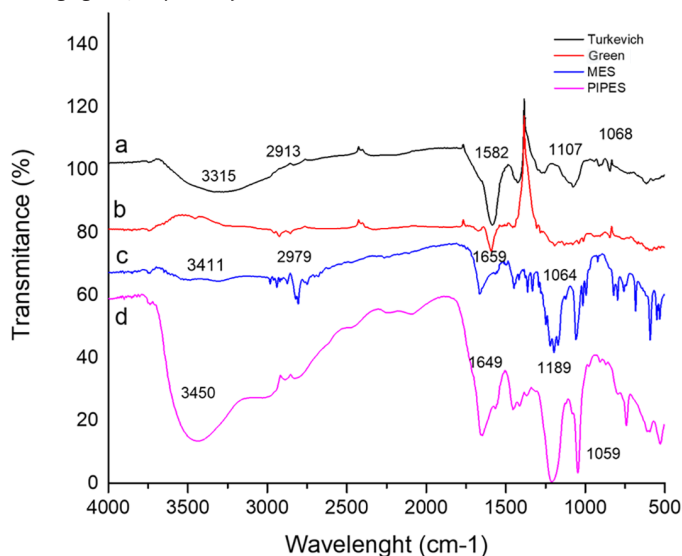
N: atomic weight of gold, 197 g/mol

The average number of gold atoms reduced by sodium citrate to form gold nanoparticles was determined to be 732,766 for Turkevich and 530,661 for the green synthesis. For the synthesis using Good's buffer method with MES and PIPES as reducing agents, 2,552,248 and 1,633,406 atoms were obtained, respectively. These data provide information on which method can produce more gold atoms per nanoparticle. In this case, Good's buffer method yielded more atoms than Turkevich and the green method, but these atoms formed larger nanoparticles due to aggregation.

FT-IR

The IR analysis of nanoparticle synthesis obtained through the Turkevich, green, and Good's buffer methods was conducted to identify nanoparticle formation through the functional groups of the reducing agents. Figure 9a

FIGURE 9. IR spectrum of gold nanoparticles synthesized by Turkevich, green and Good's buffer method. a) IR spectrum of the nanoparticles obtained by Turkevich; b) IR of the nanoparticles obtained by green method; c) and d) shows nanoparticles obtained by the Good's buffer method using MES and PIPES as reducing agents, respectively.



Source: Author's elaboration.

shows the characteristic spectrum of nanoparticles synthesized by the Turkevich method, whose absorption bands indicate that some citrate ions are attached to the nanoparticles as they exhibit an infrared spectrum with characteristic citrate bands (3315, 2913, 1582 cm^{-1}).

Thus, the stretching of the O-H bond corresponds to the band at 3315 cm^{-1} , while the band observed at 2913 cm^{-1} is related to the stretching signal

of the C-H bond corresponding to the citrate backbone. The absorption bands at 1582 cm^{-1} correspond to the stretching of the carbonyl group (C = O). Finally, the bands at 1107 and 1068 cm^{-1} represent oscillations between C-O (Giri *et al.*, 2010).

The IR spectrum in figure 9b shows bands corresponding to the synthesis of nanoparticles using the green method. The characteristic band of the aryl ketonic C = O stretching of quercetin was observed at 1659 cm^{-1} (Catauro *et al.*, 2015). Figures 9c and 9d depict the IR spectra obtained for nanoparticles synthesized using Good's buffer method with MES and PIPES as reducing agents. In figure 9c, the spectrum for synthesis with MES as a reducing agent is presented, where bands at 3411, 2979, and 1059 cm^{-1} are observed. The stretching of the bond corresponding to the band at 3411 cm^{-1} may correspond to the morpholine ring of MES, while the band at 2979 cm^{-1} corresponds to the C-H bonds of the molecule's backbone. The band at 1064 cm^{-1} is related to the dual bond between S = O (Webster *et al.*, 2014). The spectrum of nanoparticles synthesized with PIPES is shown in 9d, where differences in the number of bands and signal intensity can be observed. The structure of MES is slightly different from that of PIPES, with the differences lying in the two ethanesulfonic acids in PIPES and only one in MES. Therefore, the bands appear in regions very similar to those obtained in the MES spectrum, corresponding to vibrations of the same functional groups. Some differences lie in the intensity of the bands; for example, the band at 3450 cm^{-1} corresponds to the vibration of the OH functional group, the band at 1059 cm^{-1} corresponds to the S = O vibration, and the band at 1189 cm^{-1} may correspond to the vibration of the C-N bond (Webster *et al.*, 2014).

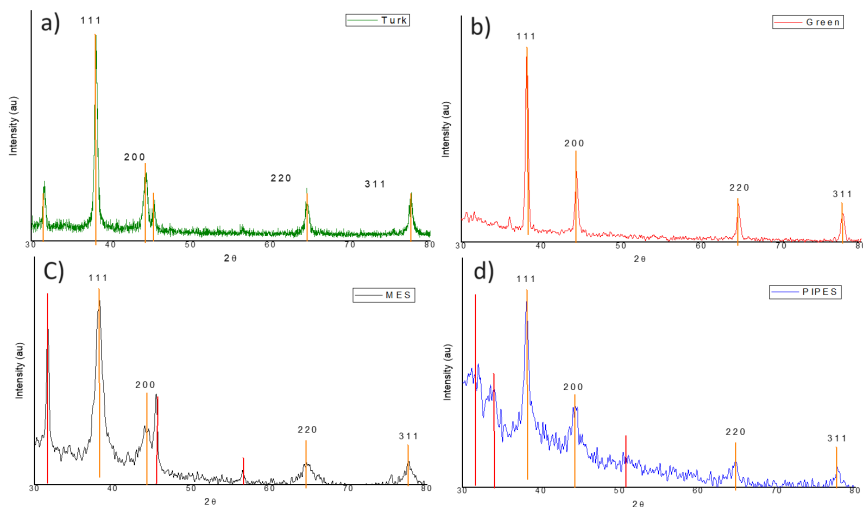
X-ray diffraction

X-ray diffraction (XRD) analysis allowed the identification of compounds present in the different syntheses obtained by three methods, and their diffraction pattern are shown in figure 10. The diffractogram (figure 10a) shows that the nanoparticles obtained by Turkevich have a crystalline cubic pattern. Thus, peaks at 111 (38.28°), 200 (44.21°), 220 (64.62°), and 311 (77.4°) corresponding to Bragg reflection confirm the fcc structure of the gold nanoparticles (figure 10a). The broadening of the Bragg peaks indicates the formation of nanoparticles (Narayanan and Sakthivel, 2008). The adjacent peaks correspond to organic compounds in the chains of the reducing agent interacting with chloroauric acid to form salts (NaCl).

Regarding figure 10b for nanoparticles synthesized using the green method, there are no peaks apart from those corresponding to Au mentioned earlier, indicating that this synthesis method efficiently reduces to Au0 and produces clean nanoparticles free of residues.

Figures 10c and 10d show Good's buffer method with MES and PIPES as reducing agents, respectively. In both diffractograms, small adjacent peaks corresponding to the formation of secondary organic compounds

FIGURE 10. XRD of gold nanoparticles synthesized by a) Turkevich, b) green method and Good's buffer method, c) MES, and, d) PIPES as reducing agent.



Source: Author's elaboration.

during the synthesis reaction are observed (Narayanan and Sakthivel, 2008). The peak intensity for this method is lower than that obtained by Turkevich and the green method, which may result from the purity of the solution obtained.

In XRD, as the size of the nanoparticles decreases, the intensity of the peaks will also decrease because there will be a smaller number of diffracting crystalline planes and there will be a greater proportion of atoms on the surface that have no order. These may be some residues of the reducing agent that serve as ligands, which reduces the diffraction of the nanoparticle, thus decreasing the crystalline order. When the size is very small, the peaks tend to be wider and with less definition indicating that perhaps the material analyzed is amorphous. It is observed in diffractograms thin peaks with definition only PIPES and MES samples have wider peaks than Turkevich and Green diffractograms and this confirms that nanoparticles are related with peaks in size and shape because PIPES and MES have non spherical shape.

Conclusions

In this work, the synthesis of gold nanoparticles was carried out using three different methodologies: Turkevich, green, and Good's buffer. The nanoparticles were characterized using UV-Vis, TEM, Z Potential, DLS, FT-IR, and X-ray diffraction techniques. The results showed that all three techniques formed nanoparticles with average sizes ranging from 20 to 43 nm. The

Turkevich method produced nanoparticles of 28.7 nm with greater uniformity in shape and size compared to the other methods. Meanwhile, the green method yielded smaller nanoparticles, with average diameters of 20 nm obtained using DLS; however, TEM imaging revealed particles as small as 1.4 nm, which cannot be detected by DLS due to the technique's resolution limitations. The green method exhibited the highest particle size dispersion (PDI = 0.61), attributed to the reducing agent used in this method, which is a flavonol. Good's buffer method, a relatively new methodology, resulted in larger nanoparticles than those synthesized by Turkevich and the green method. The morphology of the nanoparticles is not completely spherical as it is with Turkevich. Therefore, it is concluded that the three methodologies proposed in this article result in nanoparticles with characteristics that can be used in various fields of study. Depending on the application of the nanoparticles, which methodology will lead to nanoparticles with a certain surface area can be evaluated.

Conflicts of interest

The authors declare no conflicts of interest.

Authors contribution

Fátima del Rosario Balderas-Vázquez: methodological development, data mining, analysis and interpretation, writing of the original draft.

Diego A. Bravo-Alfaro: methodological development, data mining, analysis and interpretation, writing of the original draft.

Sandra Herrera-Pérez: methodological development.

Micael Gerardo Bravo-Sánchez: final review and editing of the text.

Héctor Pool: concept and design of the article.

Noé Arjona: concept and design of the article, review and final editing of the text.

Gabriel Luna-Bárceñas: concept and design of the article, data mining, analysis and interpretation, writing of the original draft.

Francisco Villaseñor-Ortega: concept and design of the article, data mining, analysis and interpretation, writing of the original draft.

References

- Abraham, M. E. and Acree, W. E. (2014). On the solubility of quercetin. *J. Mol. Liq.*, 197: 157-159. <https://doi.org/10.1016/j.molliq.2014.05.006>.
- Ahmed, S. R., Oh, S., Baba, R., Zhou, H., Hwang, S., Lee, J. and Park, E. Y. (2016). Synthesis of gold nanoparticles with buffer-dependent variations of size and morphology in biological buffers. *Nanoscale Res. Lett.*, 11: 65. <https://doi.org/10.1186/s11671-016-1290-3>.

- Bhattacharjee, S. (2016). DLS and zeta potential – What they are and what they are not? *J. Control. Release.*, 235: 337-351. <https://doi.org/10.1016/j.jconrel.2016.06.017>.
- Catauro, M., Papale, F., Bollino, F., Piccolella, S., Marciano, S., Nocera, P. and Pacifico, S. (2015). Silica/quercetin sol-gel hybrids as antioxidant dental implant materials. *Sci. technol. adv. material Meth.*, 16: 035001. <https://doi.org/10.1088/1468-6996/16/3/035001>.
- Danaei, M., Dehghankhold, M., Ataei, S., Hasanzadeh Davarani, F., Javanmard, R., Dokhani, A. and Mozafari, M. (2018). Impact of particle size and polydispersity index on the clinical applications of lipidic nanocarrier systems. *Pharmaceutics*, 10: 57. <https://doi.org/10.3390/pharmaceutics10020057>.
- Devendiran, R. M., Chinnaiyan, S. K., Yadav, N. K., Ramanathan, G., Singaravelu, S., Perumal, P. T. and Sivagnanam, U. T. (2016). Facile synthesis and evaluation of quercetin reduced and dextran sulphate stabilized gold nanoparticles decorated with folic acid for active targeting against breast cancer. *RSC Advances*, 39: 1-14. <https://doi.org/10.1039/C6RA01756H>.
- Dreaden, E. C., Alkilany, A. M., Huang, X., Murphy, C. J. and El-Sayed, M. A. (2012). The golden age: gold nanoparticles for biomedicine. *Chem. Soc. Rev.*, 41: 2740-2779. <https://doi.org/10.1039/c1cs15237h>.
- Ghosh, S. K. and Pal, T. (2007). Interparticle coupling effect on the surface plasmon resonance of gold nanoparticles: from theory to applications. *Chem. Rev.*, 107: 4797-4862. <https://doi.org/10.1021/cr0680282>.
- Giri, A., Makhil, A., Ghosh, B., Raychaudhuri, A. K. and Pal, S. K. (2010). Functionalization of manganite nanoparticles and their interaction with biologically relevant small ligands: picosecond time-resolved FRET studies. *Nanoescale*, 2: 2704-2709. <https://doi.org/10.1039/C0NR00490A>.
- Good, N. E., Douglas, W. G., Wilhelmina, W., Connolly, T. N., Izawa, S. and Singh, R. M. M. (1966). Hydrogen ion buffers for biological research. *Biochemistry*, 5: 467-477. <https://doi.org/10.1021/bi00866a011>.
- Huang, X. and El-Sayed, M. A. (2010). Gold nanoparticles: optical properties and implementations in cancer diagnosis and photo-thermal therapy. *J. Adv. Res.*, 1: 13-28. <https://doi.org/10.1016/j.jare.2010.02.002>.
- Jain, P. K., Huang, X., El-Sayed, I. H. and El-Sayed, M. A. (2007). Review of some interesting surface plasmon resonance-enhanced properties of noble metal nanoparticles and their applications to biosystems. *Plasmonics*, 2: 107-118. <https://doi.org/10.1007/s11468-007-9031-1>.
- Jain, P. K., Lee, K. S., El-Sayed, I. H. and El-Sayed, M. A. (2006). Calculated absorption and scattering properties of gold nanoparticles of different size, shape, and composition: applications in biological imaging and biomedicine. *J. Phys. Chem. B.*, 110: 7238-7248. <https://doi.org/10.1021/jp057170o>.
- Jamkhande, P. G., Ghule, N. W., Bamer, A. H. and Kalaskar, M. G. (2019). Metal nanoparticles synthesis: an overview on methods of preparation, advantages and disadvantages, and applications. *J. Drug Deliv. Sci. Technol.*, 53: 101174. <https://doi.org/10.1016/j.jddst.2019.101174>.
- Jana, N. R., Gearheart, L. and Murphy, C. J. (2001). Seed-mediated growth approach for

- shape-controlled synthesis of spheroidal and rod-like gold nanoparticles using a surfactant template. *Adv. Mater.*, 13: 1389-1393. [https://doi.org/10.1002/1521-4095\(200109\)13:18<1389::AID-ADMA1389>3.0.CO;2-F](https://doi.org/10.1002/1521-4095(200109)13:18<1389::AID-ADMA1389>3.0.CO;2-F).
- Kettemann, F., Birnbaum, A., Witte, S., Wuithschick, M., Pinna, N., Kraehnert, R., Rademann, K. and Polte, J. (2016). Missing piece of the mechanism of the turkevich method: the critical role of citrate protonation. *Chem. Mater.*, 28: 4072-4081. <https://doi.org/10.1021/acs.chemmater.6b01796>.
- Khan, I., Saeed, K. and Khan, I. (2019). Nanoparticles: properties, applications and toxicities. *Arab. J. Chem.*, 12: 908-931. <https://doi.org/10.1016/j.arabjc.2017.05.011>.
- Krajczewski, J., Kołataj, K. and Kudelski, A. (2017). Plasmonic nanoparticles in chemical analysis. *RSC Adv.*, 7: 17559-17576. <https://doi.org/10.1039/C7RA01034F>.
- Meyers, M. A., Mishra, A. and Benson, D. J. (2006). Mechanical properties of nanocrystalline materials. *Prog. Mater. Sci.*, 51, 427-556. <https://doi.org/10.1016/j.pmatsci.2005.08.003>.
- Millstone, J. E., Hurst, S. J., Metraux, G. S. and Mirkin, C. A. (2009). Colloidal gold and silver triangular nanoprisms. *Small*, 5: 646-664. <https://doi.org/10.1002/sml.200801480>.
- Mulvaney, P. (1996). Surface plasmon spectroscopy of nanosized metal particles. *Langmuir*, 12: 788-800. <https://doi.org/10.1021/la9502711>.
- Murphy, C. J., Sau, T. K., Gole, A. M., Orendorff, C. J., Gao, J., Gou, L. and El-Sayed, M. A. (2005). Anisotropic metal nanoparticles: synthesis, assembly, and optical applications. *J. Phys. Chem. B.*, 109: 13857-13870. <https://doi.org/10.1021/jp0516846>.
- Nakatuka, Y., Yoshida, H., Fukui, K. and Matuzawa, M. (2015). The effect of particle size distribution on effective zeta-potential by use of the sedimentation method. *Adv. Powder. Technol.*, 26: 650-656. <https://doi.org/10.1016/j.apt.2015.01.017>.
- Narayanan, K. B. and Sakthivel, N. (2008). Coriander leaf mediated biosynthesis of gold nanoparticles. *Mater. Lett.*, 62: 4588-4590. <https://doi.org/10.1016/j.matlet.2008.08.044>.
- Niu, J., Zhu, T. and Liu, Z. (2007). One-step seed-mediated growth of 30-150 nm quasi-spherical gold nanoparticles with 2-mercaptosuccinic acid as a new reducing agent. *Nanotechnology*, 18: 3256. <https://doi.org/10.1088/0957-4484/18/32/325607>.
- Oliveira, A. E. F., Pereira, A. C., Resende, M. A. C. and Ferreira, L. F. (2023). Gold nanoparticles: a didactic step-by-step of the synthesis using the Turkevich method, mechanisms, and characterizations. *Analytica*, 4: 250-263. <https://doi.org/10.3390/analytica4020020>.
- Pacioni, N. L., Borsarelli, C. D., Rey, V. and Veglia, A. V. (2015). Synthetic routes for the preparation of silver nanoparticles. In Alarcon, E., Griffith, M., Udekwu K. (eds.), *Silver nanoparticle applications, engineering materials*. Springer, Cham., 13-46. https://doi.org/10.1007/978-3-319-11262-6_2.
- Patel, V. R. and Agrawal, Y. K. (2011). Nanosuspension: an approach to enhance solubility of drugs. *J. Adv. Pharm. Technol. Res.*, 2: 81-87. <https://doi.org/10.4103/2231-4040.82950>.
- Polte, J. (2015). Fundamental growth principles of colloidal metal nanoparticles – A new perspective. *Cryst. Eng. Comm.*, 17: 6809-6830. <https://doi.org/10.1039/>

C5CE01014D.

- Rahme, K. and Holmes, J. D. (2015). Gold nanoparticles: synthesis, characterization, and bioconjugation. In *Dekker Encyclopedia of Nanoscience and Nanotechnology*. 3: 1-11. CRC Press.
- Scholl, J., Koh, A. and Dionne, J. (2012). Quantum plasmon resonances of individual metallic nanoparticles. *Nature*, 483: 421-427. <https://doi.org/10.1038/nature10904>.
- Szunerits, S., Spadavecchia, J. and Boukherroub, R. (2014). Surface plasmon resonance: signal amplification using colloidal gold nanoparticles for enhanced sensitivity. *Rev. Anal. Chem.* 33: 153-164. <https://doi.org/10.1515/revac-2014-0011>.
- Turkevich, J., Stevenson, P. C. and Hillier, J. (1951). A study of the nucleation and growth processes in the synthesis of colloidal gold. *Discussions of the Faraday Society*, 11: 55-75. <https://doi.org/10.1039/DF9511100055>.
- Vergara-Castañeda, H., Granados-Segura, L., Luna-Bárceñas, G., McClements, D. J., Herrera-Hernández, M. G., Arjona, N., Hernández-Martínez, A. R., Estevez, M. and Pool, H. (2019). Gold nanoparticles bioreduced by natural extracts of arantho (*Kalanchoe daigremontiana*) for biological purposes: physicochemical, antioxidant and antiproliferative evaluations. *Mater. Res. Express*, 6: 055010. <https://doi.org/10.1088/2053-1591/ab0155>.
- Wang, N., Cheng, X., Li, N., Wang, H. and Chen, H. (2019). Nanocarriers and their loading strategies. *Adv. Healthc. Mater.* 8: 1801002. <https://doi.org/10.1002/adhm.201801002>.
- Webster, F. X., Kiemle, D. J., Silverstein, R. M. and Bryce, D. L. (2014). *Spectrometric identification of organic compounds*. 8th ed. Wiley.
- Zuki, N. M., Ismail, N. and Omar, F. M. (2019). Evaluation of zeta potential and particle size measurements of multiple coagulants in semiconductor wastewater. *AIP Conference Proceedings*, 2124: 020036. <https://doi.org/10.1063/1.5117096>.